EFFECT OF INTERNAL PORES ON PROPERTIES OF CASTABLE REFRACTORIES

Yoshihiro SASATANI*, Keisuke YAMADA and Katsumi MORIKAWA

Krosaki Harima Corporation

ABSTRACT

When water is added to the powder of castable refractories and mixed with water, air is entrapped and remains as internal pores in the casted body after curing, which may affect the durability. Therefore, it is important to clarify the relationship between the pores inside the body and the physical properties. Recently, X-ray CT, which can visualize the internal structure three-dimensionally without destruction, has been actively applied to refractories. Therefore, in this report, we investigated the pores inside the body of alumina-silica castable refractories by X-ray CT and analyzed the relationship with various physical properties.

INTRODUCTION

When water is added to the powder of castable refractories and mixed with water, air is entrapped and remains as internal pores in the casted body after curing. Also, the internal structure of the same material after curing varies depending on the amount of added water.

In this study, we investigated the apparent porosity and pore diameter distribution in alumina-silica castables with variable amount of added water. In addition, for relatively coarse pores (bubbles), X-ray CT was used to analyze the bubbles inside the body[1, 2]. From these obtained data, the pore and bubble size (0.01 μm to 3 mm in diameter) distribution of each castable was measured. Also, slag infiltration resistance of each castable was investigated and correlated with the pore and bubble size distributions.

EXPERIMENT AND DISCUSSION

Table I shows a summary of the alumina-silica castables evaluated. The amount of water added was adjusted to each dispersant to obtain appropriate flow. Dispersant α is a phosphate dispersant. Dispersants β, γ, and δ are polymeric dispersants, and their dispersing ability varies depending on their molecular structure. By using different dispersants, the added water content during material casting was varied.

Table I. Test materials.

/ mass%		A	B	C	D
+1mm	Mullite, Andalusite		40		
0.1〜1mm	Andalusite		29		
-0.1mm	Alumina		○		
	Andalusite		○		
	*CAC		○		
	Silica fume		○		
	Others		○		
Dispersant types		α	β	γ	δ
Water		6.5	6.0	5.0	4.3

*CAC : Calcium Aluminate Cement

Apparent porosity was measured on samples dried at 110°C for 24 hours after curing for 24 hours. The experimental results are shown in Table II. There is a correlation between the added water content and the apparent porosity.

Table II. Properties of castables.

	A	B	C	D
Dispersant types	α	β	γ	δ
Water / mass%	6.5	6.0	5.0	4.3
Apparent porosity / %	15.4	15.3	11.9	10.7
Bulk density /	2.54	2.58	2.66	2.68

Next, pore diameter distribution was investigated. Evaluation samples were made by processing the product after drying at 110°C for 24 hours into 15 x 15 x 10 mm. The pore diameter was measured using a mercury porosimeter. The cumulative pore volume fraction was obtained from the amount of mercury intruded at each measured pore diameter and the bulk density of the castable. The cumulative pore size volume fraction is shown in Fig. 1. There was a strong correlation between the amount of water added and the cumulative pore volume fraction from 500 to 0.005 μm. The results are shown in Fig. 2. Differential pore volume distributions are shown in Fig. 3. Castable A, in which phosphate dispersant α was used, has many pores of 1 to 10 μm. In addition, the pores of castables are shifted to the fine side by using dispersants with high dispersing ability and low added water content.
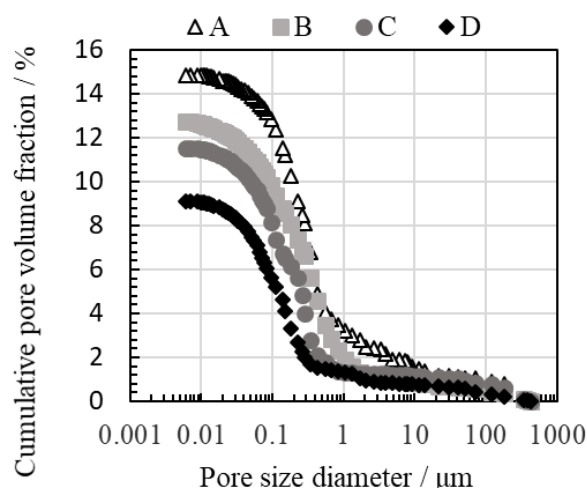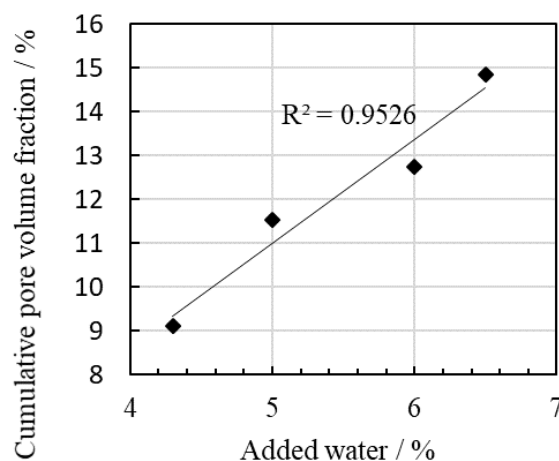

Fig. 1. Cumulative pore size distribution.

Fig. 2. Relationship cumulative pore volume fraction and added water.
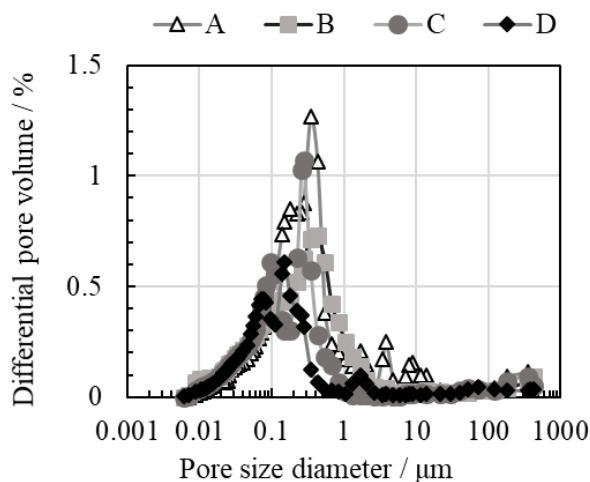

Fig. 3. Differential pore volume distributions.

Next, internal microstructure of each castable was then imaged with X-ray CT and analyzed for bubbles (pores with a diameter of 0.1 mm or more were defined as bubbles). The mercury intrusion method described above can measure pores of 0.1 to 400 μm, but not larger pores or bubbles. In this study, we attempted to observe pores and bubbles of ≥100 μm by X-ray CT.

Fig. 4 shows the scheme of an X-ray system. The tomographic image was acquired by transmitting X-rays emitted from the generator through the castable on the rotating stage and projecting a two-dimensional image on the X-ray detector placed behind. The pore structure was visualized by extracting the pore area based on the obtained tomographic image and performing three-dimensional configuration.
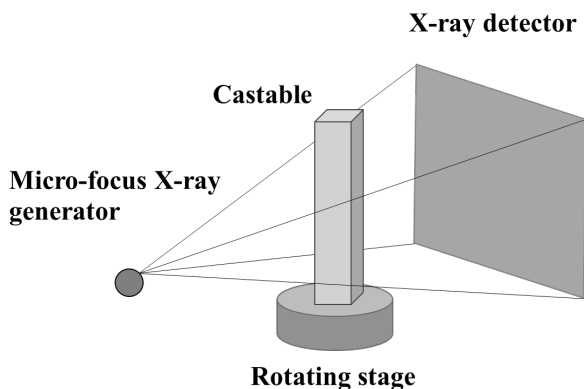

Fig. 4. Schematic image of 3D X-ray CT system.

Fig. 5 (a) shows a tomographic image of Castable A taken with the X-ray CT system. The black dots are bubbles. Fig. 5 (b) shows an image in which only the bubbles are extracted by selecting a threshold value based on the difference in luminance and performing the binarization process. Fig. 5(c) shows the result of reconstruction using an arbitrary continuous

tomogram processed as shown above. By using X-ray CT, bubbles inside the castable can be visualized in three dimensions.
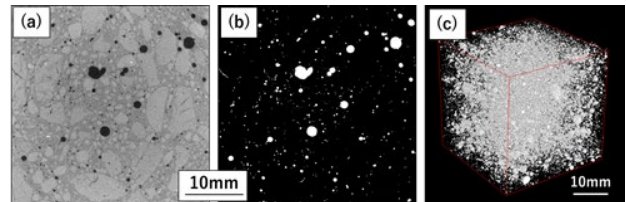

Fig. 5. Image of castable A
(a) Raw image, (b) Binarized image,
(c) 3D-CT image.

The obtained bubble structure was analyzed and the bubble and bubble diameter distribution were calculated. Fig. 6 shows the cumulative bubble size distribution, and Fig. 7 shows the differential bubble size distribution. Castable D had more bubbles of ≥100μm in diameter as shown in Fig. 6 and more bubbles of ≥1mm in diameter as shown Fig. 7 than other castables. This is probably due to the fact that Castable D, which has lower water content, has higher slurry viscosity and is more likely to entrap air than Castable A and B, making it difficult for bubbles to rise from the interior. However, as shown in Fig. 8, there was no correlation between the amount of added water in each castable and the cumulative bubble volume of ≥100 μm. We thought that castables with more added water would have lower slurry viscosity and less air bubble (air) entrapment, but the results were not necessarily consistent. It was suggested that the entrapment of air bubbles was not only due to the slurry viscosity but also to other factors.
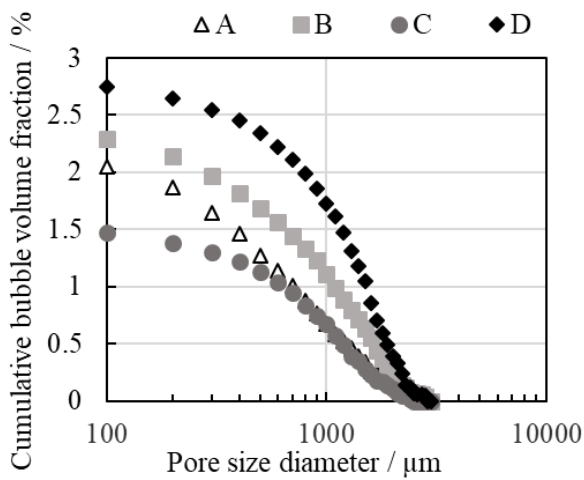
Fig. 6. Cumulative bubble size distribution obtained with X-ray CT.
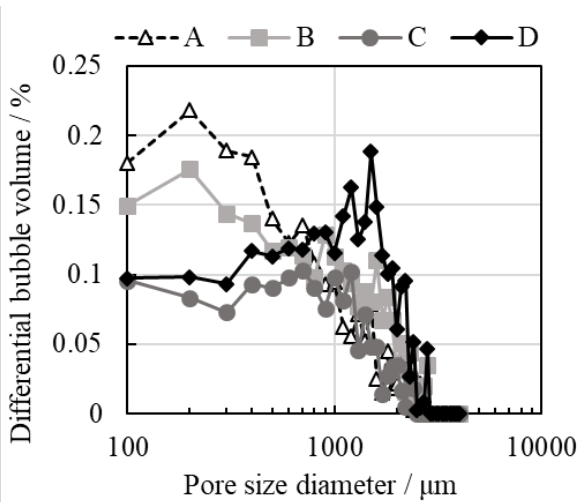

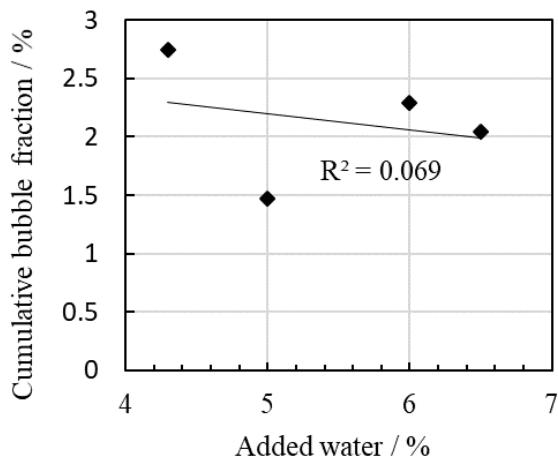Fig. 7. Differential bubble size distribution obtained with X-ray CT.

Fig. 8. Relationship cumulative bubble volume from 3000 to 100 μm and added water.

Table III summarizes the apparent porosity, the porosity of ≤400 μm measured by the mercury intrusion method, and the bubble fraction of ≥100 μm measured by X-ray CT. Those two measured data was combined and cumulative distribution plots are shown in Fig.9, and the combined frequency distribution plots are shown in Fig. 10. The pores in the castables originate from the amount of added water are concentrated in the range of 0.1-1 μm, and only Castable A has many pores around 10 μm. Bubbles of ≥400μm, which we consider to be originate from air entrainment, accounted for about 10-20% of the total pores in the castable. The maximum difference in bubble volume among the samples was about 1.2%.

In this study, by combining the results of pore size distribution measurement by mercury intrusion method and bubble measurement by X-ray CT, a wide range of pores and bubble diameters in refractory materials could be evaluated in a unified manner.

Table III. Cumulative bubble or pore.

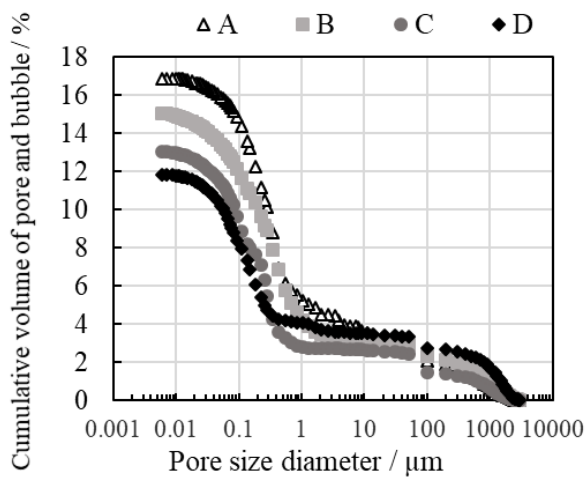|		A	B	C	D
Dispersant types		α	β	γ	δ
Water / mass%		6.5	6.0	5.0	4.3
Apparent porosity / %		15.4	15.3	11.9	10.7
*MIM	□ 400μm	14.9	12.8	11.5	9.1
X-ray CT	□ 100μm	2.0	2.3	1.5	2.7

*MIM : Mercury intrusion method

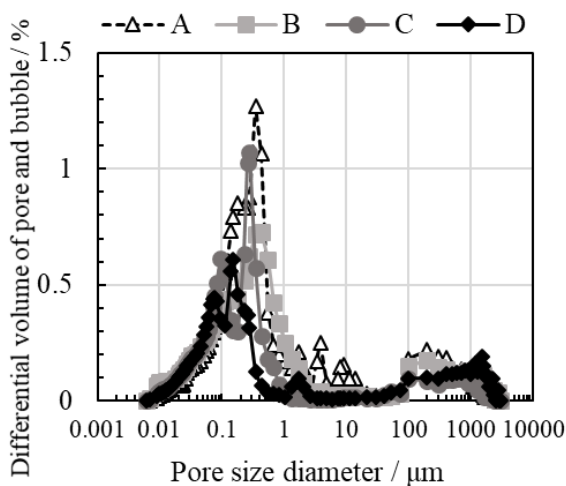Fig. 9. Cumulative pore and bubble size distribution.

Fig. 10. Differential pore and bubble size distribution.

Next, slag infiltration resistance of each castable was measured, and the correlation with pore and bubble size distribution was investigated. The slag infiltration resistance was evaluated by the crucible method. The crucible size was dia.100 x 100 with hole of dia.50 x 50mm. The crucible was pre-burned at 1400°C. After pre-burning, 40g of slag with CaO/SiO$_2$ (in mass) =3.0 was placed in the crucible and burned at 1550°C for 3h. Then, the crucible was cut in half and the slag infiltration was evaluated

by cross-sectional observation. The amount of slag infiltration is measured as the sum of the corroded area and the infiltrated area (discolored layer). The test results are shown in Fig. 11.
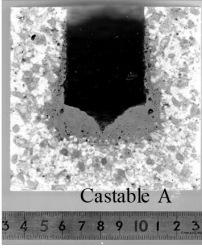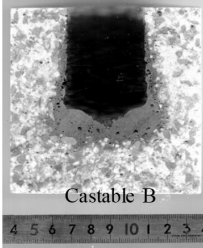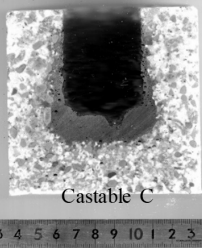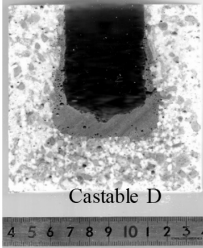
Added water / %	6.5	6
Cutting surface photo	Castable A	Castable B
Corrosion and Infiltration areas / mm^2	1176	1068
Index	100	91
Added water / %	5	4.3
Cutting surface photo	Castable C	Castable D
Corrosion and Infiltration areas / mm^2	957	847
Index	81	72

Fig. 11. Cut section of crucibles after slag infiltration test.

The relationship between the measured slag infiltration amount and the apparent porosity, the porosity of ≤400 µm measured by mercury intrusion method, and the bubble fraction of ≥100 µm measured by X-ray CT was investigated. The results are shown in Fig. 12. The amount of pores measured by the mercury intrusion method, which was highly correlated with the amount of added water, was highly correlated with the slag infiltration. The pores are ≤10µm, and the main pores are around 0.2µm, suggesting that the molten slag can

penetrate the pores by capillary action. It is clear again that reducing the water content and pores in castables is a useful method to improve the resistance to slag infiltration. The amount of bubbles (air entrapment) measured by X-ray CT did not correlate with slag infiltration. From the present results, bubbles as small as 3% (with a maximum difference of 1.2% among castables) did not have a significant effect on the slag infiltration resistance.
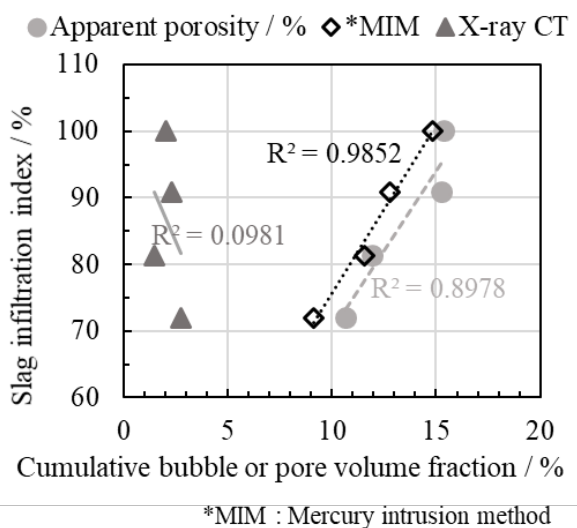

Fig. 12. Relationship slag infiltration index and cumulative bubble or pore volume fraction.

CONCLUSION

1. By combining the mercury intrusion method and X-ray CT, a wide range of pores and bubble diameters in refractory materials could be evaluated in a unified manner.
2. In this study, the pores in the castables evaluated were ≤10 μm and mainly around 0.2 μm in diameter.
3. For each castable, there was a high correlation between the pore volume in size of ≤10μm and the resistance to slag infiltration.
4. Although the amount of air bubbles in each castable varied from 1.5 to 2.7%, it did not have a significant effect on the slag infiltration resistance.

REFERENCES

1) K.Yamada, T. Oishi, S. Matsumoto, T. Ouchi, K. Gouda and K, Morikawa:Taikabutsu, 71[5](2019), 206(in Japanese).
2) T.Igata, S. Matsumoto, K. Takami and M. Shiohama:Taikabutsu, 72[2](2020), 86(in Japanese)